

Low-frequency flux noise and visualization of vortices in a $\text{YBa}_2\text{Cu}_3\text{O}_7$ dc SQUID washer with an integrated input coil

R. Straub, S. Keil, R. Kleiner

Universität Tübingen, Experimentalphysik II, D-72076 Tübingen, Germany

D. Koelle^{a)}

II. Physikalisches Institut, Universität zu Köln, D-50937 Köln, Germany

We used low-temperature scanning electron microscopy (LTSEM) for imaging quantized magnetic flux (vortices) in direct current (dc) superconducting quantum interference devices (SQUIDs) with approximately $1\text{ }\mu\text{m}$ spatial resolution at temperature $T = 77\text{ K}$ in a controllable magnetic field up to $20\text{ }\mu\text{T}$. We demonstrate that LTSEM allows to image the spatial distribution of vortices in a $\text{YBa}_2\text{Cu}_3\text{O}_7/\text{SrTiO}_3/\text{YBa}_2\text{Cu}_3\text{O}_7$ multilayer thin-film structure consisting of a dc SQUID washer with an integrated input coil on top. Simultaneously, we are able to measure the low-frequency noise of the sample under test, which allows to correlate the spatial distribution of vortices with low-frequency noise in the SQUID.

In recent years impressive progress was achieved towards the development of sensitive superconducting quantum interference devices (SQUIDs) based on high transition temperature (T_c) superconductors [1]. For high- T_c SQUID magnetometers made from epitaxially grown thin films of $\text{YBa}_2\text{Cu}_3\text{O}_7$ (YBCO) and SrTiO_3 (STO) insulating layers an rms magnetic field resolution $S_B^{1/2} < 10\text{ fT}/\sqrt{\text{Hz}}$ in the white noise limit at temperature $T = 77\text{ K}$ was reported for the best devices made so far. More typical values are some tens of $\text{fT}/\sqrt{\text{Hz}}$. Such levels of white noise are adequate for most applications of SQUIDs. Unfortunately, most devices do not achieve these low noise levels at low frequency f , say below 10-100 Hz, which makes them less suitable for many applications [1].

The main source for the excess low-frequency noise, which typically scales as $S_B \propto 1/f$, is the thermally activated vortex motion in the high- T_c thin films. This problem becomes even more serious for devices operated in magnetically unshielded environment and cooled in the earth's magnetic field, due to an increased density of fluctuating vortices. It is known that the low-frequency flux noise is correlated with the quality of the high- T_c films [2], which in turn is affected by the presence of a variety of defects in these films. However, a detailed understanding of the interplay between microstructure and noise properties of high- T_c thin films is still lacking. This hinders further improvement of the low-frequency performance of high- T_c SQUIDs and magnetometers. Furthermore, the geometry of the micropatterned devices and the patterning process itself may significantly affect their noise properties. Hence, a number of specific locations within a device may represent possible noise sources.

It is obvious, that the low-frequency noise of high- T_c SQUIDs and magnetometers depends on local properties determined by defects and geometry. Noise measurements, however, give only spatially integrated information on the device properties, which makes it difficult to locate noise sources. In this work we utilize a technique for the visualization of vortices in SQUIDs to locate possible noise sources. This technique is based on a new mode of operation of low-temperature scanning electron microscopy (LTSEM), which has been used previously for imaging the spatial distribution

of T_c or critical current density j_c in superconducting thin films and Josephson junctions and of Josephson vortices in long junctions [3]. In contrast, the LTSEM technique presented here exploits the high sensitivity of SQUIDs to magnetic flux directly. That is, we detect electron-beam-induced changes $\delta\Phi$ of the magnetic flux coupled to the SQUID loop, where the SQUID itself is the device under test. Simultaneously, we measure the low-frequency flux noise of the SQUIDs. This enables us to obtain both images of the spatial distribution of vortices and local information on noise properties of the devices under investigation.

We mount our high- T_c SQUIDs on a magnetically shielded, liquid nitrogen cooled cryostage of an SEM as described in detail in [4]. The dc SQUIDs are read out using a standard flux-locked loop (FLL) with 3.125 kHz bias current reversal to eliminate $1/f$ noise due to fluctuations in the critical current I_c of the Josephson junctions. The YBCO dc SQUIDs we have investigated so far by LTSEM yield typical levels of rms spectral density of flux noise $S_\Phi^{1/2} = 10 - 20\text{ }\mu\Phi_0/\sqrt{\text{Hz}}$ in the white noise limit at $T = 77\text{ K}$. For the spatially resolved measurements, the e-beam is used as a local perturbation which induces an increase in temperature $\delta T(x - x_0, y - y_0)$ on the sample surface (in the x - y -plane) centered around the beam spot position (x_0, y_0) . The length scale for the spatial decay of the thermal perturbation is set by the beam-electron range $R \approx 0.5\text{ }\mu\text{m}$ for a typical beam voltage $V_b = 10\text{ kV}$ [3]. This gives a maximum increase in beam induced temperature $\Delta T \approx 1\text{ K}$ at (x_0, y_0) for a typical beam current $I_b = 1\text{ nA}$. So-called $\delta\Phi$ -images are obtained by recording the e-beam induced flux change $\delta\Phi(x_0, y_0)$ as a function of the e-beam coordinates (x_0, y_0) . To improve the signal to noise ratio, we use a beam-blanking unit operating at typically 2.6 kHz and the output signal of the FLL, i.e. the e-beam induced flux change in the SQUID, is lock-in detected. This signal controls the brightness of a video screen as a function of (x_0, y_0) . Additionally, the time trace or the power spectrum of the FLL output signal can be recorded by a signal analyzer.

All measurements presented in this work were performed at $T = 77\text{ K}$ on one integrated Ketchen-type magnetome-

^{a)}e-mail: koelle@ph2.uni-koeln.de

ter based on a YBCO/STO/YBCO multilayer structure [5] with a dc SQUID square washer in the bottom YBCO and a spiral input coil in the top YBCO film, as shown in Fig. 1(a). The SQUID hole is a narrow slit, visible as a dark vertical line in Fig. 1(a), running from the center to the bottom end of the washer. At the innermost turn of the input coil a via connects both YBCO layers along the edge of the black rectangular area visible in the center of Fig. 1(a). Figure 1(b) shows a cross section of the via. The pickup loop (not shown) had been cut for investigation of the transport properties of the input coil and the via [6]. For details regarding device fabrication and geometry see [5,6].

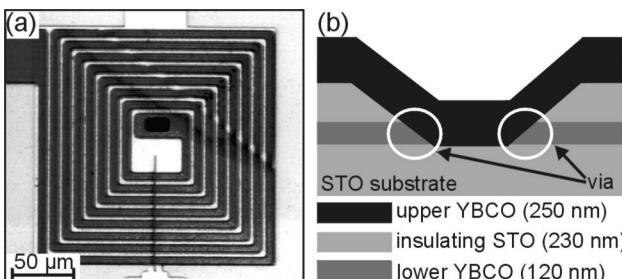


FIG. 1. (a): Optical micrograph of square washer in bottom YBCO (white) with integrated input coil in top YBCO (dark grey). (b): Sketch of cross section of the superconducting interconnect (via). The white circles indicate the location of the via edge, where top and bottom YBCO form a superconducting interconnect.

A variety of e-beam induced changes in the output signal of various YBCO dc SQUIDs has been observed and described in more detail in [7,8]. The mechanism for the imaging of vortices is also explained in [7,8] and can be briefly described as follows: The e-beam induced local increase in temperature induces a local increase in the London penetration depth λ_L . Hence, the screening currents circulating around a vortex are spatially extended due to e-beam irradiation. If the e-beam is scanned across a vortex this vortex will be dragged along with the beam, i.e. it will be displaced by some distance δr , if the beam spot is within the radial distance R from the vortex. This displacement will couple a positive (negative) flux change $\delta\Phi$ to the SQUID if the vortex is moved away from (towards) the SQUID hole.

Fig. 2(a) shows an example of a $\delta\Phi$ -image with approximately 50 vortices appearing as pairs of positive (bright) and negative (dark) signals. This image was taken from the center of the device after cooling in a static magnetic field $B_0 = 20 \mu\text{T}$ from above T_c to $T = 77\text{K}$. The maximum displacement Δr of a vortex is of the order of the change in λ_L (typically $\sim 20 \text{ nm}$ in our experiments at 77 K). This maximum displacement Δr induces a maximum signal $\Delta\Phi = (\partial\Phi/\partial r)\Delta r \equiv \phi_r(r)\Delta r$, with r being the radial distance of the vortex from the SQUID hole. As Δr is fixed for fixed I_b , V_b and T , the signal $\Delta\Phi$ is a direct measure of the coupling strength ϕ_r of an imaged vortex. Together with ϕ_r , the vortex signal $\Delta\Phi$ decreases rapidly with increasing r [9,10]. Hence, only vortices within a radial distance of some 10 μm give strong signals. An important advantage of our imaging technique, however, is the fact that the spectral density of

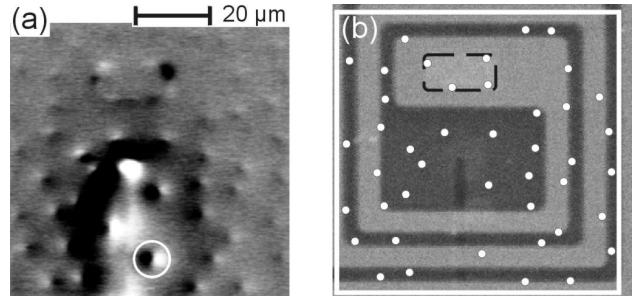


FIG. 2. (a) $\delta\Phi$ -image of central part of the device shown in Fig. 1 ($B_0 = 20 \mu\text{T}$); the white circle indicates position of a particular vortex mentioned in the discussion of Fig. 3; (b): SEM micrograph of central part of the device with the two innermost turns of the input coil (light grey); the black dashed frame indicates the position of the via. The white frame corresponds to the frame of the $\delta\Phi$ -image shown in (a). The white dots indicate positions of vortices as imaged in (a).

flux noise S_Φ induced by motion of a single vortex is given by $S_\Phi = S_r \cdot \phi_r^2$, with S_r being the spectral density of radial motion of this vortex. Therefore, measuring ϕ_r directly gives important information on possible noise sources in the investigated devices. This is particularly important for complex structures, as the one described in this letter, for which calculation of $\phi_r(x, y)$ is not straightforward.

The correlation of $\delta\Phi$ -images with surface micrographs provides information on the position of individual vortices. For this purpose we marked the position of vortices obtained from Fig. 2(a) as white dots in Fig. 2(b) (surface micrograph). We find that most vortices are located between the turns of the input coil and hence are penetrating only the lower YBCO film. This observation implies, that the 7 μm wide input coil is narrow enough to prevent entry of most vortices [11], at least up to $B_0 = 20 \mu\text{T}$. We observe a tendency of the vortices being located close to the edge of the input coil. We have not clarified yet whether this is due to preferential pinning at the edges. Alternatively, this may be due to a slightly higher T_c of the upper YBCO as compared to the bottom YBCO film [6]: Screening currents induced upon cooling the upper YBCO film through T_c in a field B_0 create an inhomogeneous flux density distribution in the bottom YBCO film with enhanced flux density near the edges of the input coil, which may favor nucleation of vortices there. Possibly for similar reasons, we always observe vortices to be located right at the via edge which is indicated as a dashed frame in Fig. 2(b). As shown previously [6], the upper YBCO film inside this frame has the highest T_c of this structure. In Fig. 2 we see four vortices pinned at the via edge, three of them exactly in the corners of the rectangle. We note that these four vortices give signals which are spatially more extended as compared to other vortices. This could be due to an increased value of λ_L at the via edge, related to reduced screening, in accordance with reduced critical current density measured for our vias [5]. However, due to the complex geometry of the via edge, which involves c-axis transport, interpretation of these signals is not straightforward. In addition these vortex signals are also stronger than from other vortices at similar r . It is not clear yet, whether this indicates a higher mobility of these vortices, which in turn would make them strong candidates for prominent low-frequency noise sources.

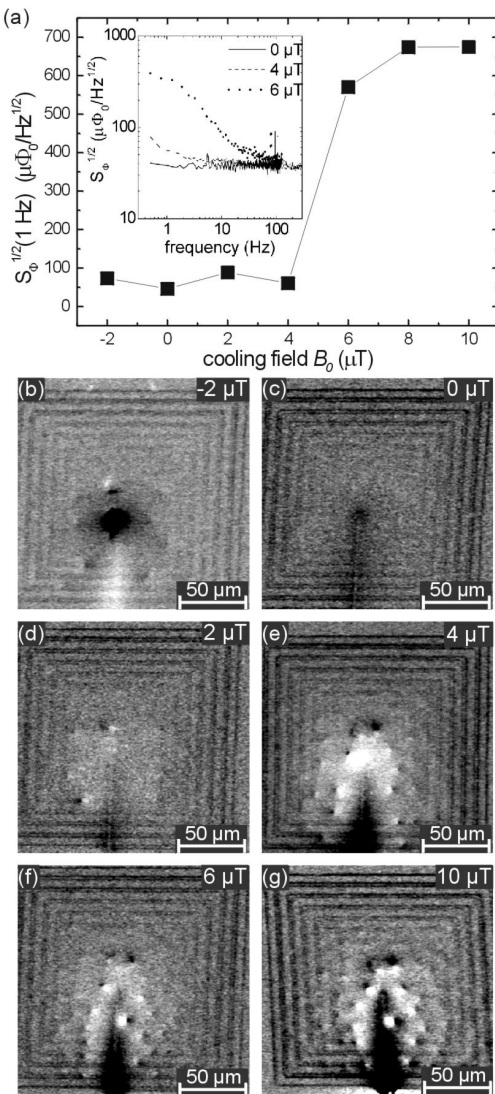


FIG. 3. Low-frequency noise and $\delta\Phi$ -images: (a) rms spectral density of flux noise $S_\Phi^{1/2}$ at $f = 1$ Hz vs. cooling field B_0 . The inset shows $S_\Phi^{1/2}(f)$ for selected values of B_0 ; (b)-(g): $\delta\Phi$ -images, taken directly before or after measuring S_Φ .

To correlate the frequently observed increase of low-frequency flux noise for increasing cooling field B_0 with the spatial distribution of vortices we took a series of $\delta\Phi$ -images from our device and measured its spectral density of flux noise directly before or after taking the image for a series of values of B_0 in the range $-2 \mu\text{T} \leq B_0 \leq 10 \mu\text{T}$. Fig. 3(a) shows the flux noise vs. cooling field measured at $f = 1$ Hz with a pronounced increase in $S_\Phi(1\text{Hz})$ above $B_0 = 4 \mu\text{T}$. For $B_0 = 0 \mu\text{T}$ the noise spectrum shown in the inset of Fig. 3(a) is white down to below $f = 1$ Hz. This corresponds to the observation of no vortices in Fig. 3(c) and the lowest value for $S_\Phi(1\text{Hz})$ in Fig. 3(a). For $B_0 = -2 \mu\text{T}$ a few vortices appear [c.f. Fig. 3(b)] which induce a slight increase in low frequency noise [c.f. Fig. 3(a)]. The situation is similar for $B_0 = 2 \mu\text{T}$, with opposite polarity of the vortices as shown in Fig. 3(d). Increasing B_0 to $4 \mu\text{T}$ increases the number of vortices [c.f. Fig. 3(e)], however, without a significant change in the low-frequency noise [c.f. Fig. 3(a)]

and inset].

At $B_0 = 6 \mu\text{T}$ a jump in the noise power by almost two orders of magnitude occurs, which comes along with the appearance of one particular vortex located [c.f. Fig. 2(a)] at the second innermost turn, close to the place where the turn crosses over the slit in the SQUID washer. This location has previously been identified to have the lowest I_c in our structure [6]. The noise spectrum [c.f. inset of Fig. 3(a)] is of Lorentzian-type which indicates that it is dominated by a single strong fluctuator. Moreover, we took images in the same cooling field $B_0 = 6 \mu\text{T}$ which did not show occupation of this particular site with a vortex. In those cases the low frequency noise was low and comparable to the values obtained for $B_0 \leq 4 \mu\text{T}$. This suggests strongly that the large increase in low frequency flux noise at $B_0 = 6 \mu\text{T}$ is due to the presence of this single fluctuating vortex.

In conclusion, we demonstrated that LTSEM provides images of the spatial distribution of vortices pinned in a high- T_c dc SQUID multilayer magnetometer. The combination of vortex imaging with low frequency noise measurements enabled us to identify a single vortex being responsible for a large excess low-frequency flux noise in the device under test. In general, the combination of vortex imaging and low-frequency noise measurements in variable magnetic field is expected to give new insights into the mechanisms which are responsible for generation of the frequently observed high levels of flux noise in high- T_c SQUIDs and magnetometers.

We thank John Clarke and G. Nichols for providing detailed layouts of their SQUID-readout electronics. The integrated magnetometer was fabricated at UC Berkeley. We gratefully acknowledge collaboration with F. Ludwig, E. Dantsker, A. H. Miklich, D. T. Nemeth and John Clarke who provided this device. This work was supported by the Deutsche Forschungsgemeinschaft (Hu251/27-1, Gr1132/11-1) and the ESF VORTEX program.

- [1] D. Koelle, R. Kleiner, F. Ludwig, E. Dantsker, J. Clarke, Rev. Mod. Phys. **71**, 631 (1999); **71**, 1249 (E) (1999).
- [2] M. J. Ferrari, M. Johnson, F.C. Wellstood, J.J. Kingston, T.J. Shaw, J. Clarke, J. Low Temp. Phys. **94**, 15 (1994).
- [3] R. Gross and D. Koelle, Rep. Prog. Phys. **57**, 651 (1994).
- [4] R. Gerber, T. Nissel, H.-G. Wener, A. Willmann, R.P. Huebener, D. Koelle, R. Gross, Cryogenics **37**, 21 (1997); R. Gerber, D. Koelle, T. Nissel, R. Gross, R.P. Huebener, IEEE Trans. Appl. Supercond. **7**, 3231 (1997).
- [5] F. Ludwig, D. Koelle, E. Dantsker, D.T. Nemeth, A.H. Miklich, J. Clarke, R.E. Thomson, Appl. Phys. Lett. **66**, 373 (1995); F. Ludwig, E. Dantsker, D. Koelle, R. Kleiner, A.H. Miklich, D.T. Nemeth, J. Clarke, D. Drung, S. Knappe, H. Koch, IEEE Trans. Appl. Supercond. **5**, 2919 (1995).
- [6] R. Gerber, D. Koelle, R. Gross, R.P. Huebener, F. Ludwig, E. Dantsker, R. Kleiner, J. Clarke, Appl. Phys. Lett. **68**, 1555 (1996).
- [7] S. Keil, R. Straub, R. Gerber, R.P. Huebener, D. Koelle, R. Gross, K. Barthel, IEEE Trans. Appl. Supercond. **9**, 2961 (1999).
- [8] D. Koelle, R. Gross, R. Straub, S. Keil, M. Fischer, M. Peschka, R.P. Huebener, K. Barthel, Physica C **332**, 148 (2000).
- [9] M. J. Ferrari, J. J. Kingston, F. C. Wellstood, J. Clarke, Appl. Phys. Lett. **58**, 1106 (1991).
- [10] R. G. Humphreys, IEEE Trans. Appl. Supercond. **9**, 3741 (1999).
- [11] E. Dantsker, S. Tanaka, J. Clarke, Appl. Phys. Lett. **70**, 2037 (1997).